East European Journal of Physics. 4. 393–404 (2024)
DOI: 10.26565/2312-4334-2024-4-46 ISSN 2312-4334

NUMERICAL STUDY ON THE EFFECTS OF THERMAL AND MASS STRATIFICATION ON CHEMICALLY REACTING UNSTEADY MHD NANOFLUID PAST AN OSCILLATING VERTICAL PLATE THROUGH A POROUS MEDIUM

Hemant Agarwal[a], **Shyamanta Chakraborty**[b], **Rupam Shankar Nath**[a]
[a] *Department of Mathematics, Gauhati University,Guwahati-781014, Assam, India*
[b] *UGC-HRDC, Gauhati University, Guwahati-781014, Assam, India*
[*] *Corresponding Author e-mail: hemantagarwal55@gmail.com*
Received July 22, 2024; revised October 6, 2024; accepted October 14, 2024

The purpose of this study is to study the combined influence of thermal and mass stratification on unsteady magnetohydrodynamic nanofluid past a vertically oscillating plate with variable temperature. The problem's governing equations are numerically solved using the implicit Crank-Nicolson approach. Significant results from the thermal and mass stratification are contrasted with the environment where stratification is absent. The velocity decreases with both kinds of stratification, while the temperature decreases with thermal stratification and the concentration decreases with mass stratification. We use graphs to demonstrate the effects of the different parameters, including phase angle, thermal radiation, magnetic field strength, heat sources/sinks, and chemical reactions. Additionally, the Skin-Friction Coefficient, the Nusselt Number, and the Sherwood Number are computed and represented graphically. The findings highlight the critical role of stratification in improving fluid dynamics and increasing the efficiency of heat and mass transfer processes, providing essential information for engineering and environmental applications under similar circumstances.

Keywords: *Mass Stratification; Chemical Reaction; Nanofluid; Thermal Stratification; Oscillating Vertical Plate; Crank-Nicolson Method; Thermal Radiation; Porous Medium; MHD*

PACS: 44.05.+e, 44.25.+f, 44.27.+g, 44.40.+a, 47.11.-j, 44.30.+v

1. INTRODUCTION

The term "nanofluid" is used to describe a specific form of artificial fluid in which particles with sizes typically less than 100 nanometers are suspended in a base fluid. The unique thermal and mechanical features of nanofluids have attracted a lot of attention in recent years, leading to their widespread implementation. One of the most promising applications in the field of heat transfer is the use of nanofluids, which perform better than their base fluids in terms of both thermal conductivity and convective heat transfer coefficients. They are helpful in a range of heat transfer applications, such as solar collectors, heat exchangers, and the cooling of electronic devices, thanks to their capacity to dissipate heat effectively.

Choi and Eastman [1] was the first to introduce the concept of nanofluid, which indicates that floating metallic nanoparticles in standard heat transfer fluids could create a revolutionary novel kind of heat transmission fluid. In a partly heated rectangular enclosure, Oztop and Abu-Nada [2] conducted a numerical investigation on several kinds of nanoparticles and how they impact on heat transmission and fluid flow. The authors of the papers Das and Jana [3] and [4] examined the radiation-induced free convection flow of nanofluids in a vertical plate and channel, respectively. Titanium dioxide, aluminium oxide, and copper nanofluids were the subject of investigation in both reports. The study conducted by Rashidi et al. [5] investigates the utilisation of lie group theory to provide a solution for the movement of nanofluid across a chemically reactive horizontal plate, considering the generation or absorption of heat. The study conducted by Abolbashari et al. [6] applies the homotopy analysis method (HAM) to examine the entropy of the nanofluid composed of water as the fundamental fluid and member of four different kinds of nanoparticles: TiO_2, Al_2O_3, Cu, and CuO. The nanofluid past over a stretched permeable surface. Kameswaran et al. [7] studied the impact of several factors on convection heat and mass transfer in nanofluid move across a stretching sheet, including the viscous dissipation, soret effect, hydro-magnetic, chemical reaction, and viscous dissipation. For the purpose of exploring the impact of certain factors, a numerical study was carried out by Motsumi and Makinde [8] on the flow via the boundary layer of nanofluids over a movable flat plate. The study aimed to analyze the consequence of viscous dissipation, thermal diffusion, and thermal radiation. Furthermore, Sheikholeslami et al. [9] examined the flow of MHD nanofluids numerically to determine the impact of viscous loss on the flow. As it move via a upright plate, Chamkha and Aly [10] numerically evaluates an MHD nanofluid that has heat production or absorption impacts. The analytical examination on the MHD nanofluid movement for different types of water-based nanoparticles as they travelled through a continuously stretching/shrinking permeable sheet was conducted by Turkyilmazoglu [11] within the framework of velocity slip and temperature leap. A circular tube was used to perform experimental study on a diluted CuO/water nanofluid by Fotukian et al. [12]. In their research of the MHD Cu-water nanofluid subjected to Lorentz forces, Sheikholeslami et al. [13] utilised the Lattice Boltzmann method. In addition, Sandeep and Reddy [14] investigated the influences of nonlinear thermal radiation on

Cite as: H. Agarwal, S. Chakraborty, R.S. Nath, East Eur. J. Phys. 4, 393 (2024), https://doi.org/10.26565/2312-4334-2024-4-46

the flow of MHD Cu-water nanofluids across a cone and a wedge. The influences of mass and heat transfer on nanofluids travelling through a moving or stationary upright plate in the presence of a heat source were studied by Reddy et al. [15] and Mahanthesh et al. [16], respectively. Vemula et al. [17] performed an analytical study to examine the motion of magnetohydrodynamic (MHD) nanofluids flowing past a vertically oriented plate that is accelerating exponentially, while also having a temperature that changes. The united impacts of mass and heat stratification across an upright wavy truncated cone and a wavy surface were studied by Cheng [**?**] and [19], respectively. In addition, the impact of these effects on infinite vertical cylinders has been studied by Paul and Deka [20]. Krishna et al. [21] studied MHD Carreau fluid flows, emphasizing how bouyancy and exponential heat sources modify fluid behaviour. Recent efforts by Gowri and Selvaraj [22] and Selvaraj et al. [23] have focused on rotational effects and the dynamics of accelerated flows in porous media, offering deeper insights into how rotational forces affect MHD parabolic flows. The study conducted in Nath and Deka [24] examined the impact of both temperature stratification and chemical reactions on the flow around an indefinite vertical plate. Similarly, the investigation in Kalita et al. [25] focused on the influence of these factors on the flow around an accelerated upright plate and Nath et al. [26], conducted a study on how thermal stratification affects the flow of unstable parabolic motion around a upright plate that extends infinitely. Nath and Deka [27] conducted a study on how heat and mass stratification affect the movement of an unstable magnetohydrodynamic nanofluid across an upright plate. The plate's temperature varies exponentially, and the study was conducted in a porous media. In a similar vein, Nath and Deka [28] investigated numerically how temperature and mass stratification affect the flow of a magnetohydrodynamic nanofluid that is unstable as it passes across a porous medium with an exponentially accelerating upright plate. An endless upright plate with a temperature that drops exponentially and changing mass diffusion in a porous medium was studied by Nath and Deka [29] in terms of the effect on temperature and mass stratification. The MHD ternary hybrid nanofluid was the subject of a numerical study by Nath and Deka [30]. The study revolved around a cylinder that was stretched vertically within a porous medium that had heat stratification and radiation. The study conducted by Sheikholeslami et al. [31] examined the influence of the diffusion of heat and heat generation on the erratic multi-channel hydrodynamics (MHD) flow of a radiatively and electrically conducting nanofluid passing through a porous medium across an oscillating upright plate. Rammoorthi and Mohanavel [32] looked into how a magnetic field's radiation can affect the convective movement of a reactive chemically hybrid nanofluid across an upright plate.

In this work, we investigate the behavior of an unsteady MHD nanofluid in a porous media as it flows through an oscillating vertical plate with variable temperature. The unique aspects of this particular problem are as follows: It makes use of a numerical method that is both efficient and unconditionally stable, and it guarantees convergence with ease. So far, no one has tried to show how mass and temperature stratification work together to affect MHD nanofluid as it circulates across a porous medium with ramping temperature and concentration, past an oscillating vertical plate. Nanoparticles of Ag-water and Cu-water was studied for how thermal and mass stratification affected them in the occurrence of a magnetic field(M), thermal radiation(R), heat generation or absorption(Q), and chemical reaction(Kr). As far as we know, no attempt has ever been made to carry out this kind of research. Nanofluid stratification research is a promising and rapidly expanding field with potential applications in medical technology, catalysis, and energy storage.

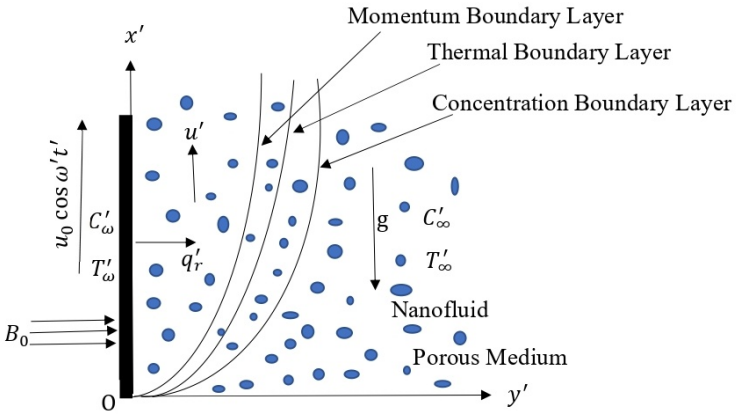

Figure 1. Physical Model and Coordinate System

2. MATHEMATICAL FORMULATION

Examine the transfer of heat and flow in nanofluids as they pass an oscillating vertical plate with changing temperature. The flow is erratic, viscous, incompressible, and exhibits free convection. The x' axis is oriented vertically and parallel to the surface of the plate, while the magnetic field is oriented perpendicular to the direction of propagation with the y' axis. The initial assumption is that the surrounding nanofluid and the plate have the same temperature and concentration,

denoted as T'_∞ and C'_∞ accordingly. At $t' > 0$, the plate starts to oscillate vertically inside its own plane at a frequency of ω'. Simultaneously, the temperature exhibits a linear increase over time, while the concentration is denoted as C'_w. The plate is assumed to be exposed to a uniform magnetic field B_0, and the heat produced by viscous and joule dissipation is not taken into account. It is crucial to analyze the radiative heat flux that is perpendicular to the direction of the plate, which is represented by the symbol q'_r. Our work will focus on the analysis of a water-based nanofluid including nanoparticles of silver (Ag) and copper (Cu). The governing equations of momentum, energy, and concentration for nanofluid given by authors in Mahanthesh et al. [16] and Vemula et al. [17] using the boundary layer approximation and Boussinesq are written as

$$\begin{aligned}\rho_{nf}\frac{\partial u'}{\partial t'} &= \mu_{nf}\frac{\partial^2 u'}{\partial y'^2} + g(\rho\beta_T)_{nf}(T'-T'_\infty) + g(\rho\beta_C)_{nf}(C'-C'_\infty) - \sigma_{nf}B_0^2 u' \\ &\quad -\frac{\mu_{nf}}{k'_p}u' \qquad (1)\\ \frac{\partial T'}{\partial t'} &= \frac{k_{nf}}{(\rho c_p)_{nf}}\frac{\partial^2 T'}{\partial y'^2} - \frac{1}{(\rho c_p)_{nf}}\frac{\partial q'_r}{\partial y'} + \frac{Q_0}{(\rho c_p)_{nf}}(T'-T'_\infty) - \gamma u' \qquad (2)\\ \frac{\partial C'}{\partial t'} &= D_{nf}\frac{\partial^2 C'}{\partial y'^2} - k_1(C'-C'_\infty) - \xi u' \qquad (3)\end{aligned}$$

The initial and boundary conditions are as follows:

$u' = 0$	$T' = T'_\infty$	$C' = C'_\infty$	$\forall y', t' \le 0$
$u' = u_0 \cos\omega' t'$	$T' = T'_\infty + (T'_w - T'_\infty)At'$	$C' = C'_w$	at $y' = 0, t' > 0$
$u' = 0$	$T' \to T'_\infty$	$C' \to C'_\infty$	as $y' \to \infty, t' > 0$

where, $(\beta_T)_{nf}, (\beta_C)_{nf}, \rho_{nf}, \mu_{nf}, \sigma_{nf}, B_0, g, k'_p, k_{nf}, (\rho c_p)_{nf}, Q_0, q'_r, D_{nf}, k_1$ denote the thermal expansion coefficient of the nanofluid, coefficient of expansion for species concentration of the nanofluid, the density of the nanofluid, dynamic viscosity of the nanofluid, electrical conductivity of the nanofluid, uniform magnetic field, acceleration due to gravity, porous medium permeability, thermal conductivity of the nanofluid, heat capacitance of the nanofluid, uniform volumetric heat source/sink, radiative heat flux, mass diffusion coefficient of the nanofluid, chemical reaction coefficient respectively. Moreover, the "thermal stratification parameter" and "mass stratification parameter" are denoted as $\gamma = \frac{dT'_\infty}{dx'} + \frac{g}{C_p}$ and $\xi = \frac{dC'_\infty}{dx'}$ respectively. The concept of "thermal stratification" encompasses the phenomenon of vertical temperature advection, denoted as $\left(\frac{dT'_\infty}{dx'}\right)$, wherein the temperature of the surrounding fluid varies with height, and work of compression, denoted as $\left(\frac{g}{C_p}\right)$, which represents the rate at which reversible work is performed on fluid particles through compression. The mathematical representations of certain physical quantities are in the following manner:

$$\mu_{nf} = \frac{\mu_f}{(1-\phi)^{2.5}}, \quad \rho_{nf} = (1-\phi)\rho_f + \phi\rho_s, \quad (\rho c_p)_{nf} = (1-\phi)(\rho c_p)_f + \phi(\rho c_p)_s$$

$$(\rho\beta_T)_{nf} = (1-\phi)(\rho\beta_T)_f + \phi(\rho\beta_T)_s, \quad (\rho\beta_C)_{nf} = (1-\phi)(\rho\beta_C)_f + \phi(\rho\beta_C)_s$$

$$\sigma = \frac{\sigma_s}{\sigma_f}, \quad \sigma_{nf} = \left[1 + \frac{3\phi(\sigma-1)}{(\sigma+2) - \phi(\sigma-1)}\right]\sigma_f, \quad k_{nf} = \left[\frac{(k_s+2k_f) - 2\phi(k_f-k_s)}{(k_s+2k_f) + \phi(k_f-k_s)}\right]k_f$$

where $\rho_s, \rho_f, \mu_f, \phi, (\rho c_p)_s, (\rho c_p)_f, \sigma_f, k_s, k_f$ denote the density of nanoparticles, density of base fluid, viscosity of base fluid, volume fraction of nanoparticle, heat capacitance of nanoparticles, heat capacitance of base fluid, electrical conductivity of nanoparticles, thermal conductivity of nanoparticles and thermal conductivity of base fluid respectively. The Rosseland estimate [33] is used to get a good idea of the flux of radiative heat q'_r in Eq. (2), since the nanofluid is thought to be an optically thick fluid. According to the study by Turkyilmazoglu [11], we can rewrite Eq. (2) as

$$\frac{\partial T'}{\partial t'} = \frac{1}{(\rho c_p)_{nf}}\left(k_{nf} + \frac{16\sigma^* T'^3_\infty}{3k_f k}\right)\frac{\partial^2 T'}{\partial y'^2} + \frac{Q_0}{(\rho c_p)_{nf}}(T'-T'_\infty) - \gamma u'$$

Now, we provide the subsequent non-dimensional quantities:

$$U = \frac{u'}{u_0}, \quad t = \frac{t' u_0^2}{\nu_f}, \quad y = \frac{y' u_0}{\nu_f} = \frac{y'}{L_{ref}}, \quad \theta = \frac{T'-T'_\infty}{T'_w - T'_\infty}, \quad C = \frac{C'-C'_\infty}{C'_w - C'_\infty}, \quad M = \frac{\nu_f \sigma_f B_0^2}{\rho_f u_0^2}$$

$$Gr = \frac{g\beta_{T_f}\nu_f(T'_w - T'_\infty)}{u_0^3}, \quad Gc = \frac{g\beta_{C_f}\nu_f(C'_w - C'_\infty)}{u_0^3}, \quad Pr = \frac{(\mu c_p)_f}{k_f}, \quad Sc = \frac{\nu_f}{D_{nf}}, \quad R = \frac{k_f k'}{4\sigma^* T'^3_\infty},$$

$$\omega = \frac{\omega'\nu_f}{u_0^2}, \quad Q = \frac{Q_0\nu_f}{u_0^2(\rho c_p)_f}, \quad K = \frac{u_0^2 k'_p}{\nu_f^2}, \quad Kr = \frac{\nu_f k_1}{u_0^2}, \quad S = \frac{\gamma\nu_f}{u_0(T'_w - T'_\infty)}, \quad F = \frac{\xi\nu_f}{u_0(C'_w - C'_\infty)}$$

The non-dimensional forms of the Eq. (1)-(3) are given by

$$\frac{\partial U}{\partial t} = a_1\frac{\partial^2 U}{\partial y^2} + a_2 Gr\theta + a_3 GcC - a_4 MU - a_1\frac{U}{K} \tag{4}$$

$$\frac{\partial \theta}{\partial t} = a_5\frac{\partial^2 \theta}{\partial y^2} + a_6\theta - SU \tag{5}$$

$$\frac{\partial C}{\partial t} = \frac{1}{Sc}\frac{\partial^2 C}{\partial y^2} - KrC - FU \tag{6}$$

where,

$$x_1 = (1-\phi) + \phi\left(\frac{\rho_s}{\rho_f}\right), \quad x_2 = (1-\phi) + \phi\frac{(\rho\beta_T)_s}{(\rho\beta_T)_f}, \quad x_3 = (1-\phi) + \phi\frac{(\rho\beta_C)_s}{(\rho\beta_C)_f}$$

$$x_4 = 1 + \frac{3\phi(\sigma-1)}{(\sigma+2) - \phi(\sigma-1)}, \quad x_5 = (1-\phi) + \phi\frac{(\rho C_p)_s}{(\rho C_p)_f}, \quad x_6 = \frac{(k_s + 2k_f) - 2\phi(k_f - k_s)}{(k_s + 2k_f) + \phi(k_f - k_s)}$$

$$a_1 = \frac{1}{(1-\phi)^{2.5}x_1}, \quad a_2 = \frac{x_2}{x_1}, \quad a_3 = \frac{x_3}{x_1}, \quad a_4 = \frac{x_4}{x_1}, \quad a_5 = \frac{x_6 + \frac{4}{3R}}{x_5 Pr}, \quad a_6 = \frac{Q}{x_5}$$

Non-dimensional form of initial and boundary conditions are:

$$\begin{array}{llll} U = 0 & \theta = 0 & C = 0 & \forall y, t \le 0 \\ U = \cos\omega t & \theta = t & C = 1 & \text{at } y = 0, t > 0 \\ U = 0 & \theta \to 0 & C \to 0 & \text{as } y \to \infty, t > 0 \end{array} \tag{7}$$

Table 1. Thermo-physical properties of water and nanoparticles [16]

Physical Properties	H_2O(base fluid)	Ag	Cu
$\rho\ (kg/m^3)$	997.1	10500	8933
$C_p\ (J/kgK)$	4179	235	385
$k\ (W/mK)$	0.613	429	401
$\beta_t \times 10^6\ (K^{-1})$	210	18.9	16.7
$\beta_c \times 10^6\ (K^{-1})$	214	56.7	50.1
$\sigma\ (s/m)$	5.5×10^{-6}	63×10^6	59.6×10^6

3. METHOD OF SOLUTION

It is impossible to find the exact solutions for coupled partial differential equations Eq. (4)-(6) with initial and boundary conditions (7). Therefore, to resolve them, we employ an implicit crank-Nicolson finite difference approach. The finite difference scheme of the Eq. (4) is as follows

$$\begin{aligned} \frac{U_i^{n+1} - U_i^n}{\frac{\Delta t}{2}} &= a_1\left[\frac{U_{i-1}^{n+1} - 2U_i^{n+1} + U_{i+1}^{n+1}}{(\Delta y)^2}\right] + a_1\left[\frac{U_{i-1}^{n} - 2U_i^{n} + U_{i+1}^{n}}{(\Delta y)^2}\right] + a_2 Gr\left[\theta_i^{n+1} + \theta_i^n\right] \\ &\quad + a_3 Gc\left[C_i^{n+1} + C_i^n\right] - a_4 M\left[U_i^{n+1} + U_i^n\right] - \frac{a_1}{K}\left[U_i^{n+1} + U_i^n\right] \\ \Rightarrow U_i^{n+1} - U_i^n &= \frac{a_1\Delta t}{2(\Delta y)^2}\left[U_{i-1}^{n+1} - 2U_i^{n+1} + U_{i+1}^{n+1}\right] + \frac{a_1\Delta t}{2(\Delta y)^2}\left[U_{i-1}^{n} - 2U_i^{n} + U_{i+1}^{n}\right] \end{aligned}$$

$$
\begin{aligned}
&+\frac{a_2 Gr\Delta t}{2}\left[\theta_i^{n+1}+\theta_i^n\right]+\frac{a_3 Gc\Delta t}{2}\left[C_i^{n+1}+C_i^n\right]-\frac{a_4 M\Delta t}{2}\left[U_i^{n+1}+U_i^n\right]\\
&-\frac{a_1\Delta t}{2K}\left[U_i^{n+1}+U_i^n\right]\\
\Rightarrow U_i^{n+1}-U_i^n &= b_1\left[U_{i-1}^{n+1}-2U_i^{n+1}+U_{i+1}^{n+1}\right]+b_1\left[U_{i-1}^n-2U_i^n+U_{i+1}^n\right]+b_2\left[\theta_i^{n+1}+\theta_i^n\right]\\
&+b_3\left[C_i^{n+1}+C_i^n\right]-b_4\left[U_i^{n+1}+U_i^n\right]-b_5\left[U_i^{n+1}+U_i^n\right]
\end{aligned}
$$

$$
\begin{aligned}
\Rightarrow -b_1U_{i-1}^{n+1}+(1+2b_1+b_4+b_5)U_i^{n+1}-b_1U_{i+1}^{n+1} &= b_1U_{i-1}^n+(1-2b_1-b_4-b_5)U_i^n+b_1U_{i+1}^n\\
&+b_2\left[\theta_i^{n+1}+\theta_i^n\right]+b_3\left[C_i^{n+1}+C_i^n\right] \qquad (8)
\end{aligned}
$$

where, $b_1=\frac{a_1\Delta t}{2(\Delta y)^2}$, $b_2=\frac{a_2 Gr\Delta t}{2}$, $b_3=\frac{a_3 Gc\Delta t}{2}$, $b_4=\frac{a_4 M\Delta t}{2}$, $b_5=\frac{a_1\Delta t}{2K}$

Likewise, the finite difference scheme of the Eq. (5) can be outlined as follows

$$
\begin{aligned}
\frac{\theta_i^{n+1}-\theta_i^n}{\frac{\Delta t}{2}} &= a_5\left[\frac{\theta_{i-1}^{n+1}-2\theta_i^{n+1}+\theta_{i+1}^{n+1}}{(\Delta y)^2}\right]+a_5\left[\frac{\theta_{i-1}^n-2\theta_i^n+\theta_{i+1}^n}{(\Delta y)^2}\right]+a_6\left[\theta_i^{n+1}+\theta_i^n\right]\\
&-S\left[U_i^{n+1}+U_i^n\right]\\
\Rightarrow \theta_i^{n+1}-\theta_i^n &= \frac{a_5\Delta t}{2(\Delta y)^2}\left[\theta_{i-1}^{n+1}-2\theta_i^{n+1}+\theta_{i+1}^{n+1}\right]+\frac{a_5\Delta t}{2(\Delta y)^2}\left[\theta_{i-1}^n-2\theta_i^n+\theta_{i+1}^n\right]\\
&+\frac{a_6\Delta t}{2}\left[\theta_i^{n+1}+\theta_i^n\right]-\frac{S\Delta t}{2}\left[U_i^{n+1}+U_i^n\right]\\
\Rightarrow \theta_i^{n+1}-\theta_i^n &= b_6\left[\theta_{i-1}^{n+1}-2\theta_i^{n+1}+\theta_{i+1}^{n+1}\right]+b_6\left[\theta_{i-1}^n-2\theta_i^n+\theta_{i+1}^n\right]+b_7\left[\theta_i^{n+1}+\theta_i^n\right]\\
&-b_8\left[U_i^{n+1}+U_i^n\right]
\end{aligned}
$$

$$
\begin{aligned}
\Rightarrow -b_6\theta_{i-1}^{n+1}+(1+2b_6-b_7)\theta_i^{n+1}-b_6\theta_{i+1}^{n+1} &= b_6\theta_{i-1}^n+(1-2b_6+b_7)\theta_i^n+b_6\theta_{i+1}^n\\
&-b_8\left[U_i^{n+1}+U_i^n\right] \qquad (9)
\end{aligned}
$$

where, $b_6=\frac{a_5\Delta t}{2(\Delta y)^2}$, $b_7=\frac{a_6\Delta t}{2}$, $b_8=\frac{S\Delta t}{2}$

Also, the finite difference scheme of the Eq. (6) can be outlined as follows

$$
\begin{aligned}
\frac{C_i^{n+1}-C_i^n}{\frac{\Delta t}{2}} &= \frac{1}{Sc}\left[\frac{C_{i-1}^{n+1}-2C_i^{n+1}+C_{i+1}^{n+1}}{(\Delta y)^2}\right]+\frac{1}{Sc}\left[\frac{C_{i-1}^n-2C_i^n+C_{i+1}^n}{(\Delta y)^2}\right]-Kr\left[C_i^{n+1}+C_i^n\right]\\
&-F\left[U_i^{n+1}+U_i^n\right]\\
\Rightarrow C_i^{n+1}-C_i^n &= \frac{\Delta t}{2Sc(\Delta y)^2}\left[C_{i-1}^{n+1}-2C_i^{n+1}+C_{i+1}^{n+1}\right]+\frac{\Delta t}{2Sc(\Delta y)^2}\left[C_{i-1}^n-2C_i^n+C_{i+1}^n\right]\\
&-\frac{Kr\Delta t}{2}\left[C_i^{n+1}+C_i^n\right]-\frac{F\Delta t}{2}\left[U_i^{n+1}+U_i^n\right]\\
\Rightarrow C_i^{n+1}-C_i^n &= b_9\left[C_{i-1}^{n+1}-2C_i^{n+1}+C_{i+1}^{n+1}\right]+b_9\left[C_{i-1}^n-2C_i^n+C_{i+1}^n\right]-b_{10}\left[C_i^{n+1}+C_i^n\right]\\
&-b_{11}\left[U_i^{n+1}+U_i^n\right]
\end{aligned}
$$

$$
\begin{aligned}
\Rightarrow -b_9C_{i-1}^{n+1}+(1+2b_9+b_{10})C_i^{n+1}-b_9C_{i+1}^{n+1} &= b_9C_{i-1}^n+(1-2b_9-b_{10})C_i^n+b_9C_{i+1}^n\\
&-b_{11}\left[U_i^{n+1}+U_i^n\right] \qquad (10)
\end{aligned}
$$

where, $b_9=\frac{\Delta t}{2Sc(\Delta y)^2}$, $b_{10}=\frac{Kr\Delta t}{2}$, $b_{11}=\frac{F\Delta t}{2}$ To address the issue, a rectangular region is partitioned into an arrangement of lines that are parallel to the coordinate axes, with a spacing of Δy in space and Δt in time. In this context, the variable i denotes the spatial grid points, which are spaced out by Δy. On the other hand, the variable n represents the temporal grid points, which are separated by Δt. The mesh system being evaluated for computation has step sizes of $\Delta y = 0.01$ and $\Delta t = 0.001$. By considering the initial condition stated in Eq. (7), we obtain the following:

$$U_i^0=0, \theta_i^0=0, C_i^0=0 \quad \text{for all } i$$

Now, using the left boundary condition of Eq. (7), we get:

$$U_0^n = \cos\omega t, \theta_0^n = t, C_0^n = 1 \quad \text{for all } n$$

Similarly, using the right boundary condition of Eq. (7), we obtain:

$$U_{i_{max}}^n = 0, \theta_{i_{max}}^n = 0, C_{i_{max}}^n = 0 \quad \text{for all } n$$

The initial conditions tell us what U, θ, and C are at the 1st time level, which is on the right-hand side of equations (8)–(10). The boundary conditions tell us what U, θ, and C are at the (n+1)th time level, which is also on the right-hand side of equations (8)–(10). Using the right sides of equations (8)-(10), it is possible to derive every value from the left-hand side at the (n+1)th time level. For every unknown $(n-1)$time level, this procedure is repeated. At each internal node point on a specific (n)th level, a tridiagonal system of equations is composed of equations (8)-(10). To solve these systems of equations, the Thomas algorithm, which was devised by Carnahan et al. [34] , is employed. U, θ, and C values are thus acquired at every internal node on a unique i at the (n+1)th time level. During each time step of the calculation, the tridiagonal equations corresponding to variables U, θ, and C are resolved through iterative procedures. The procedure of iteration concludes while the estimated percentage of round-off error for two successive iterations falls within the error tolerance of 10^{-4} at all grid points. It is assumed that the outcomes for U, θ, and C have attained their steady-state value when there are no absolute differences between the values of these variables at each grid point following two consecutive time steps. The numerical technique is considered consistent due to the local truncation error, which has an order of $[(\Delta y)^2 + (\Delta t)^2]$ and approaches zero as Δy and Δt approach zero. Apart from that, Soundalgekar and Ganesan [35] proved that the implicit finite-difference approach of the Crank-Nicolson type is unconditionally stable. The convergence of the numerical scheme is guaranteed by this because of its stability and compatibility.

4. RESULT AND DISCUSSIONS

In order to acquire a comprehensive picture of the situation, we computed numerical values for many physical parameters, including velocity, temperature, concentration, skin friction, Nusselt number, and Sherwood number. These calculations were performed for varying values of the parameters $S, F, Gc, Gr, K, M, Q, R, Kr$, and the phase angle (ωt). The numerical computations were executed using MATLAB, and the results are presented in figures (3)-(17). To verify the accuracy of the numerical method used, our study is compared to one by Rajesh et al. [17], which did not account for the effects of thermal stratification and heat source. The results of the current investigation are very comparable, as illustrated in Fig. 2. Table 2 displays the findings of the Nusselt number comparison between Ag(water) and Rajesh et al. [17] for various values of ϕ and R, excluding the presence of S and Q.

In the course of the research, the following values were utilized: $S = 0.7, F = 0.7, Gr = 5, Gc = 5, M = 2, K = 5, R = 3, Q = 1, Kr = 0.3, Pr = 0.71, Sc = 0.22, \omega t = \pi/3, \phi = 0.05$ and $t = 0.7$. The combined influence of the mass stratification (F) and thermal (S) factors on the non-dimensional velocity is seen in Fig. 3. The velocity diminishes when the thermal stratification (S) and mass stratification (F) intensify. There is a decrease in the effective convective potential between the hot plate and the fluid that is surrounding it when the parameter for thermal stratification, denoted by (S), is

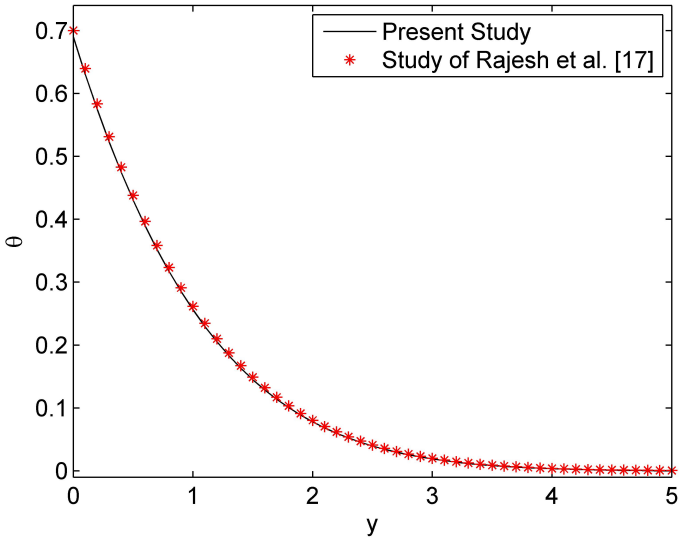

Figure 2. Comparison of the Temperature Profile without S, Q

Table 2. Comparison of Nusselt number for Ag(water) when $Pr = 6.2, t = 0.5$ and in absence of S, Q

ϕ	R	Rajesh et al. [17]	Present Study
0		1.6530	1.6523
0.01		1.6820	1.6812
0.02	3	1.7109	1.7101
0.03		1.7399	1.7391
0.04		1.7689	1.7681
	1	1.4133	1.4126
	3	1.7689	1.7681
0.04	5	1.8785	1.8777
	7	1.9322	1.9313
	9	1.9641	1.9632

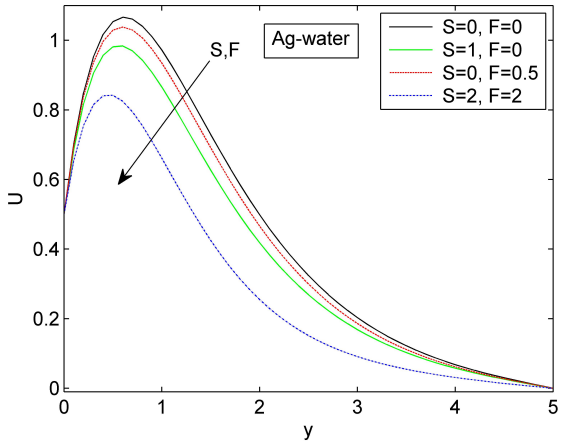

Figure 3. Velocity Profile for various values of S, F

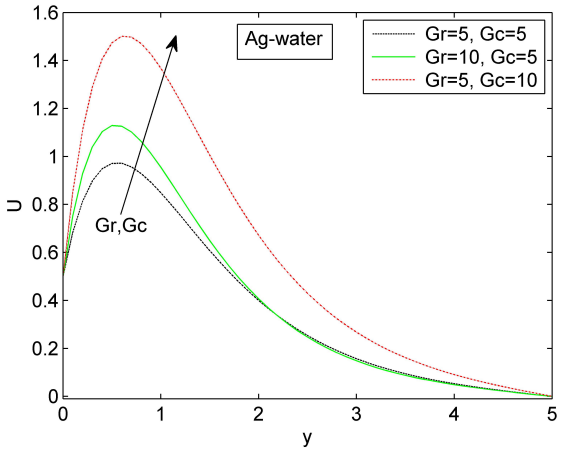

Figure 4. Velocity Profile for various values of Gr, Gc

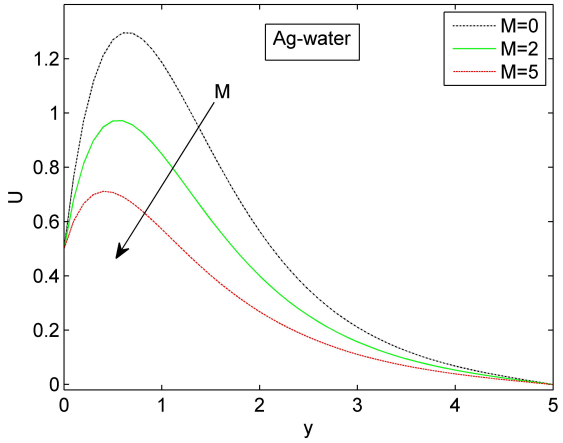

Figure 5. Velocity Profile for various values of M

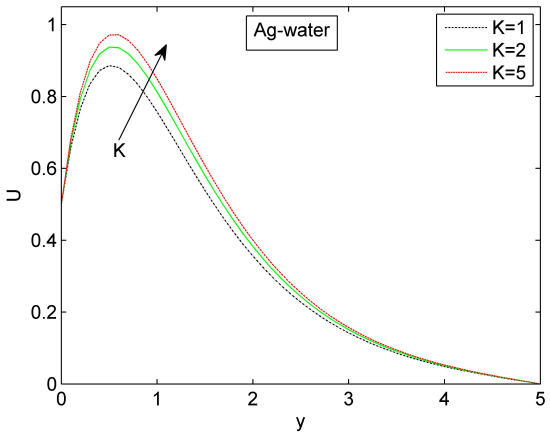

Figure 6. Velocity Profile for various values of K

increased. The buoyancy force is diminished due to this, leading to a decrease in the flow velocity. Moreover, elevating the mass stratification (F) value decreases the gradient of concentration between the surrounding environment and the surface. This leads to a decrease in the upward force exerted by the fluid, thereby causing a decrease in the velocity of the fluid flow. The velocity of the nanofluid is influenced by the combined effects of Gr and Gc, as illustrated in Fig. 4. An rise in the values of Gr and Gc leads to an increase in velocity. Increasing both Gr and Gc enhances the strength of the thermal and mass buoyancy forces. This suggests that both the thermal and mass buoyancy effects have a tendency to boost the velocity of the nanofluid. As depicted in Fig. 5, the fluid velocity diminishes with a rise in the magnetic parameter (M). It is observed that the thickness of the momentum boundary layer reduces as the magnetic parameter (M) increases. This pattern arises due to the Lorentz force generated by the transverse magnetic field, which causes a decrease

in the velocity of the nanofluid. The relationship between the porosity parameter (K) and the velocity of the nanofluid is seen in Fig. 6. The velocity is directly proportional to the value of the porosity parameter. Fig.7 demonstrates a reduction in the velocity of the nanofluid as the phase angle (ωt) increases.

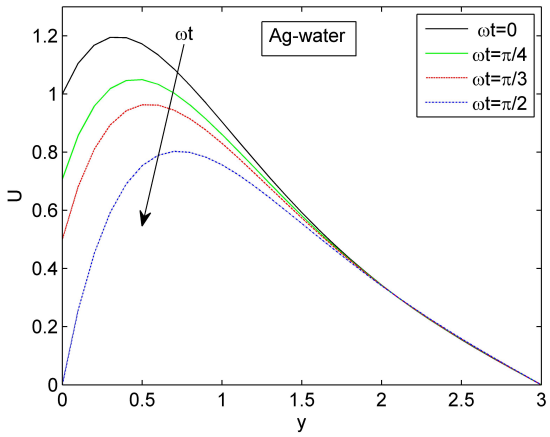

Figure 7. Velocity Profile for various values of ωt

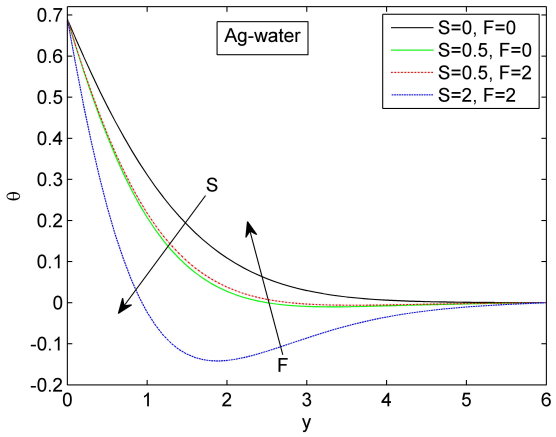

Figure 8. Temperature Profile for various values of S, F

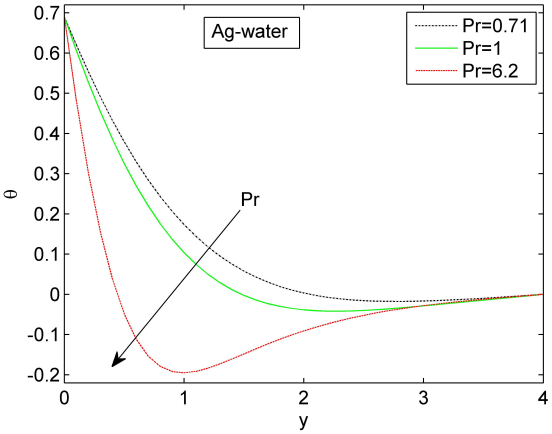

Figure 9. Temperature Profile for various values of Pr

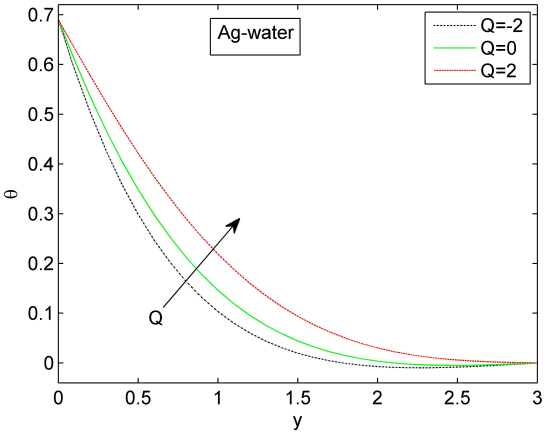

Figure 10. Temperature Profile for various values of Q

According to Fig. 8, the temperature of the nanofluid decreases with increasing thermal stratification (S) but increases with increasing mass stratification (F). The presence of thermal stratification (S) will cause a decrease in the temperature difference between the vertical plate and the surrounding fluid. As a result, the thermal boundary layer increases in thickness and the temperature decreases. It has been discovered that the boundary layer temperature will become negative for specific values of the stratification parameters (S, F). This phenomenon occurs because the fluids in close proximity to the plate may exhibit lower temperatures compared to the surrounding medium. Fig. 9 demonstrates the impact of the Prandtl number (Pr) on the temperature distribution of the nanofluid. As the Prandtl number increases, the temperature of the nanofluid decreases. A fluid with a high Prandtl number exhibits a diminished thermal conductivity. Consequently, the fluid's ability to conduct heat decreases, resulting in a decrease in the transfer rate and a reduction in the thickness of the thermal boundary layer. Therefore, the temperature of the nanofluid decreases. The influence of a heat source parameter (Q) on the temperature profile may be shown in Fig. 10. As the heat source parameter (Q) rises, the temperature of the nanofluid likewise gets higher. This characteristic corresponds to the overall physical behavior of the fluid. The temperature of the nanofluid lowers as the values of R increase in Fig. 11. This is due to the correlation between greater R values and lower thermal radiative flux, leading to lower temperatures. This can be seen as evidence of a decline in temperatures.

As seen in Fig. 12, the concentration of the nanofluid decreases as the mass stratification increases (F), while it increases when the thermal stratification occurs (S). Furthermore, Fig. 13 illustrates the impact of the Schmidt number (Sc) on the concentration profile. The concentration decreases whenever the Sc value increases. The concentration falls as the value of the chemical reaction parameter (Kr) increases, as depicted in Fig. 14. The concentration gradient is nullified due to a destructive chemical reaction, resulting in the cancellation of the buoyancy effect.

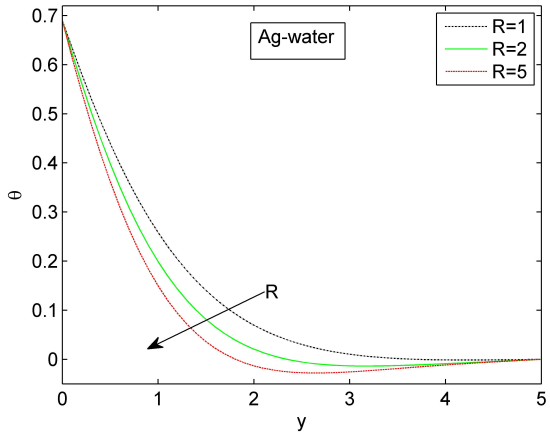

Figure 11. Temperature Profile for various values of R

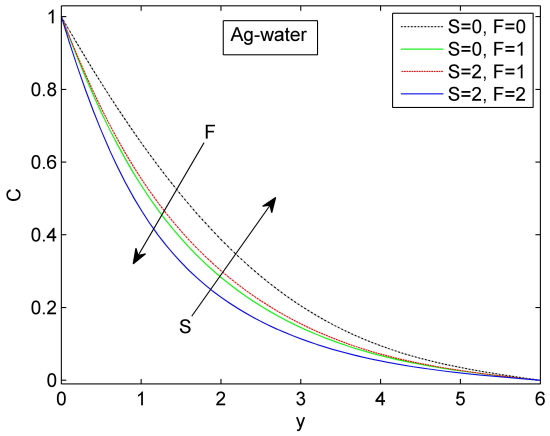

Figure 12. Concentration Profile for various values of S, F

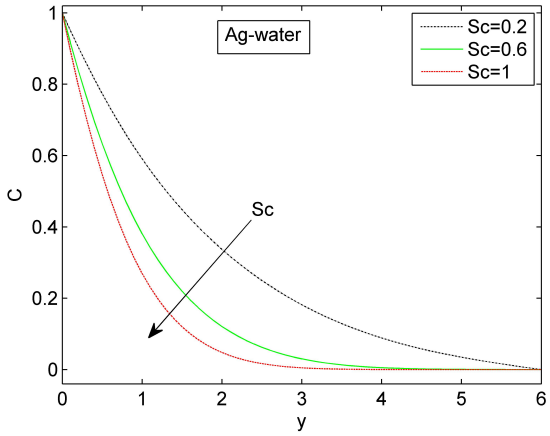

Figure 13. Concentration Profile for various values of Sc

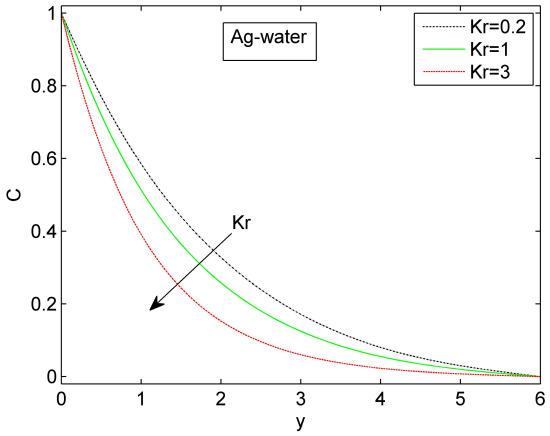

Figure 14. Concentration Profile for various values of Kr

4.1. Skin-Friction Coefficient, Nusselt Number and Sherwood Number

The skin-friction coefficient(C_f), the Nusselt number(Nu) and the Sherwood number(Sh) are defined, respectively as follows

$$C_f = \frac{\tau_w}{\rho_f u_0^2}, \quad Nu = \frac{q_w L_{ref}}{k_f(T'_W - T'_\infty)}, \quad Sh = \frac{q_m L_{ref}}{D_{nf}(C'_W - C'_\infty)}$$

where τ_w, q_w, q_m are the shear stress or skin-friction , rate of the heat flux and the rate of mass transfer from the surface of the plate correspondingly defined by

$$\tau_w = \mu_{nf}\left(\frac{\partial u'}{\partial y'}\right)_{y'=0}, \quad q_w = k_{nf}\left(\frac{\partial T'}{\partial y'}\right)_{y'=0}, \quad q_m = D_{nf}\left(\frac{\partial C'}{\partial y'}\right)_{y'=0}$$

By utilizing non-dimensional quantities, we obtain

$$C_f = \frac{1}{(1-\phi)^{2.5}}\left(\frac{\partial U}{\partial y}\right)_{y=0}, \quad Nu = -\frac{k_{nf}}{k_f}\left(\frac{\partial \theta}{\partial y}\right)_{y=0}, \quad Sh = -\left(\frac{\partial C}{\partial y}\right)_{y=0}$$

The outcomes of thermal and mass stratification parameters on the skin-friction coefficient(C_f), Nusselt number(Nu), and Sherwood number(Sh) are shown in Figures 15, 16 and 17. In both stratification, the skin-friction coefficient decreases. Without stratification, the Nusselt number would continue to decline indefinitely, but increasing mass stratification(F) and reducing thermal stratification(S) would help it to approach a stable state. Likewise, the Sherwood number obtains a stable state for greater thermal stratification(S) and lower mass stratification(F).

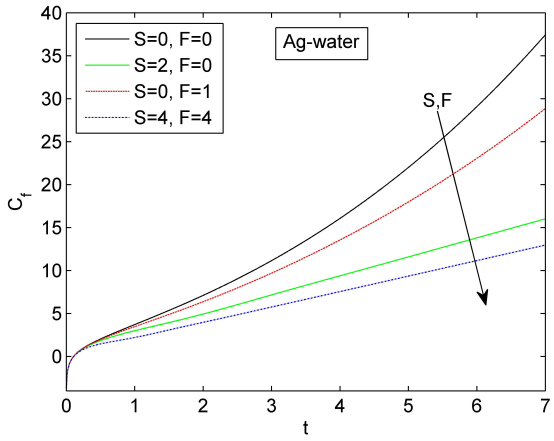

Figure 15. Skin-friction Coefficient for various values of S, F

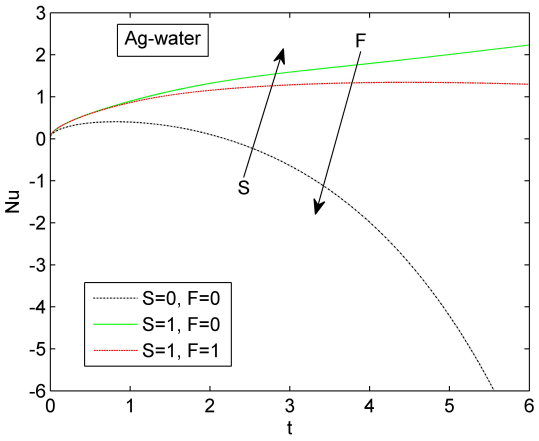

Figure 16. Nusselt Number for various values of S, F

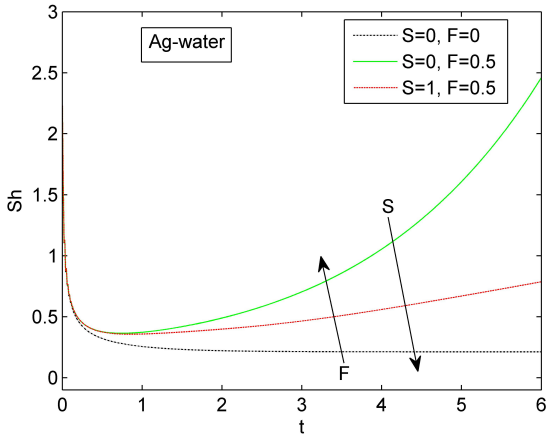

Figure 17. Sherwood Number for various values of S, F

5. CONCLUSIONS

This research paper explores the effects of thermal and mass stratification on unsteady MHD nanofluid for Ag-water and Cu-water as it pasts an oscillating vertical plate in a porous medium with variable temperature. The outcomes of this study reveal that when the thermal stratification parameter is increased, the velocity, temperature, and skin friction coefficient all decrease, but the concentration rises significantly. Moreover, A decrease in velocity, concentration, and the Nusselt number, together with an increase in temperature, are the outcomes of increasing the mass stratification parameter. The stratification significantly enhances the thermal conductivity of the nanofluid. The increased thermal conductivity enables more efficient heat transfer, making it applicable in several industries like power generation, cooling of electronic components, and manufacturing of vehicles. In numerous chemical reactions, Ag nanoparticles function as effective catalysts. They can increase reaction velocity and selectivity due to their huge surface area and distinctive electrical characteristics. Our research will help them be used to treat pollution, make chemicals, and make catalytic converters.

ORCID

Hemant Agarwal, https://orcid.org/0009-0004-2115-6482; **Shyamanta Chakraborty**, https://orcid.org/0000-0001-5839-4856; **Rupam Shankar Nath**, https://orcid.org/0009-0002-2352-0538

REFERENCES

[1] S.U.S. Choi, and J.A. Eastman, Enhancing thermal conductivity of fluids with nanoparticles. Technical report, (Argonne National Lab.(ANL), Argonne, IL, United States, 1995). https://ecotert.com/pdf/196525_From_unt-edu.pdf

[2] H.F. Oztop, and E. Abu-Nada, "Numerical study of natural convection in partially heated rectangular enclosures filled with nanofluids," International journal of heat and fluid flow, **29**(5), 1326–1336 (2008). https://doi.org/10.1016/j.ijheatfluidflow.2008.04.009

[3] S. Das, and R.N. Jana, "Natural convective magneto-nanofluid flow and radiative heat transfer past a moving vertical plate,' Alexandria Engineering Journal, **54**(1), 55–64 (2015). https://doi.org/10.1016/j.aej.2015.01.001

[4] S. Das, R.N. Jana, and O.D. Makinde, "Transient natural convection in a vertical channel filled with nanofluids in the presence of thermal radiation," Alexandria Engineering Journal, **55**(1), 253–262 (2016). https://doi.org/10.1016/j.aej.2015.10.013

[5] M.M. Rashidi, E. Momoniat, M. Ferdows, and A. Basiriparsa, "Lie group solution for free convective flow of a nanofluid past a chemically reacting horizontal plate in a porous media," Mathematical Problems in Engineering, 2014, (2014). https://doi.org/10.1155/2014/239082

[6] M.H. Abolbashari, N. Freidoonimehr, F. Nazari, and M.M. Rashidi, "Entropy analysis for an unsteady mhd flow past a stretching permeable surface in nano-fluid," Powder Technology, **267**, 256–267 (2014). https://doi.org/10.1016/j.powtec.2014.07.028

[7] P.K. Kameswaran, M. Narayana, P. Sibanda, and P.V.S.N. Murthy, "Hydromagnetic nanofluid flow due to a stretching or shrinking sheet with viscous dissipation and chemical reaction effects," International Journal of Heat and Mass Transfer, **55**(25-26), 7587–7595 (2012). https://doi.org/10.1016/j.ijheatmasstransfer.2012.07.065

[8] T.G. Motsumi, and O.D. Makinde, "Effects of thermal radiation and viscous dissipation on boundary layer flow of nanofluids over a permeable moving flat plate,' Physica Scripta, **86**(4), 045003 (2012). https://dx.doi.org/10.1088/0031-8949/86/04/045003

[9] M. Sheikholeslami, S. Abelman, and D.D. Ganji, "Numerical simulation of mhd nanofluid flow and heat transfer considering viscous dissipation," International Journal of Heat and Mass Transfer, **79**, 212–222 (2014). https://doi.org/10.1016/j.ijheatmasstransfer.2014.08.004

[10] A.J. Chamkha, and A.M. Aly, "MHD free convection flow of a nanofluid past a vertical plate in the presence of heat generation or absorption effects," Chemical Engineering Communications, **198**(3), 425–441 (2010). https://doi.org/10.1080/00986445.2010.520232

[11] M. Turkyilmazoglu, "Exact analytical solutions for heat and mass transfer of mhd slip flow in nanofluids," Chemical Engineering Science, **84**, 182–187 (2012). https://doi.org/10.1016/j.ces.2012.08.029

[12] S.M. Fotukian, and M.N. Esfahany, "Experimental study of turbulent convective heat transfer and pressure drop of dilute cuo/water nanofluid inside a circular tube," International communications in heat and mass transfer, **37**(2), 214–219 (2010). https://doi.org/10.1016/j.icheatmasstransfer.2009.10.003

[13] M. Sheikholeslami, M.G. Bandpy, R. Ellahi, and A. Zeeshan, "Simulation of MHD cuo–water nanofluid flow and convective heat transfer considering lorentz forces," Journal of Magnetism and Magnetic Materials, **369**, 69–80 (2014). https://doi.org/10.1016/j.jmmm.2014.06.017

[14] N. Sandeep, and M.G. Reddy, "Heat transfer of nonlinear radiative magnetohydrodynamic cu-water nanofluid flow over two different geometries," Journal of Molecular Liquids, **225**, 87–94 (2017). https://doi.org/10.1016/j.molliq.2016.11.026

[15] P.C. Reddy, M.C. Raju, and G.S.S. Rajum, "Free convective heat and mass transfer flow of heat-generating nanofluid past a vertical moving porous plate in a conducting field," Special Topics and Reviews in Porous Media: An International Journal, **7**(2), 2016. https://doi.org/10.1615/SpecialTopicsRevPorousMedia.2016016973

[16] B. Mahanthesh, B.J. Gireesha, and R.S.R. Gorla, "Heat and mass transfer effects on the mixed convective flow of chemically reacting nanofluid past a moving/stationary vertical plate," Alexandria engineering journal, **55**(1), 569–581 (2016). https://doi.org/10.1016/j.aej.2016.01.022

[17] R. Vemula, L. Debnath, and S. Chakrala, "Unsteady mhd free convection flow of nanofluid past an accelerated vertical plate with variable temperature and thermal radiation," International Journal of Applied and Computational Mathematics, **3**(2), 1271–1287 (2017). https://doi.org/10.1007/s40819-016-0176-5

[18] C.-Y. Cheng, "Double-diffusive natural convection along a vertical wavy truncated cone in non-newtonian fluid saturated porous media with thermal and mass stratification," International Communications in Heat and Mass Transfer, **35**(8), 985–990 (2008). https://doi.org/10.1016/j.icheatmasstransfer.2008.04.007

[19] C.-Y. Cheng, "Combined heat and mass transfer in natural convection flow from a vertical wavy surface in a power-law fluid saturated porous medium with thermal and mass stratification," International Communications in Heat and Mass Transfer, **36**(4), 351–356 (2009). https://doi.org/10.1016/j.icheatmasstransfer.2009.01.003

[20] A. Paul, R.K. Deka, et al., "Unsteady natural convection flow past an infinite cylinder with thermal and mass stratification," Int. J. Eng. Math. **2017**, 8410691 (2017). https://doi.org/10.1155/2017/8410691

[21] P.M. Krishna, N. Sandeep, and R.P. Sharma, "Computational analysis of plane and parabolic flow of mhd carreau fluid with buoyancy and exponential heat source effects," The European Physical Journal Plus, **132**, 202–216 (2017). https://doi.org/10.1140/epjp/i2017-11469-9

[22] T. Gowri, and A. Selvaraj, "Rotational effect of unsteady mhd-parabolic flow past a vertical plate through porous medium with uniform temperature mass diffusion," International Journal of Mechanical Engineering, **6**, 2468–2473 (2021). https://www.kalaharijournals.com/resources/DEC_337.pdf

[23] A. Selvaraj, S.D. Jose, R. Muthucumaraswamy, and S. Karthikeyan, "MHD-parabolic flow past an accelerated isothermal vertical plate with heat and mass diffusion in the presence of rotation," Materials Today: Proceedings, **46**, 3546–3549 (2021). https://doi.org/10.1016/j.matpr.2020.12.499

[24] R.S. Nath, and R.K. Deka, "The effects of thermal stratification on flow past an infinite vertical plate in presence of chemical reaction," East European Journal of Physics, (3), 223–232 (2023). https://doi.org/10.26565/2312-4334-2023-3-19

[25] N. Kalita, R.K. Deka, and R.S. Nath, "Unsteady flow past an accelerated vertical plate with variable temperature in presence of thermal stratification and chemical reaction," East European Journal of Physics, (3), 441–450 (2023). https://doi.org/10.26565/2312-4334-2023-3-49

[26] R.S. Nath, R.K. Deka, and H. Kumar, "The effect of thermal stratification on unsteady parabolic flow past an infinite vertical plate with chemical reaction," East European Journal of Physics, (4), 77–86 (2023). https://doi.org/10.26565/2312-4334-2023-4-08

[27] R.S. Nath, and R.K. Deka, "Theoretical study of thermal and mass stratification effects on mhd nanofluid past an exponentially accelerated vertical plate in a porous medium in presence of heat source, thermal radiation and chemical reaction," International Journal of Applied and Computational Mathematics, **10**(2), 92 (2024). https://doi.org/10.1007/s40819-024-01721-9

[28] R.S. Nath, and R.K. Deka, "Thermal and mass stratification effects on MHD nanofluid past an exponentially accelerated vertical plate through a porous medium with thermal radiation and heat source," International Journal of Modern Physics B, 2550045 (2024). https://doi.org/10.1142/S0217979225500456

[29] R.S. Nath, and R.K. Deka, "Thermal and mass stratification effects on unsteady parabolic flow past an infinite vertical plate with exponential decaying temperature and variable mass diffusion in porous medium," ZAMM-Journal of Applied Mathematics and Mechanics/Zeitschrift für Angewandte Mathematik und Mechanik, **104**(6), e202300475 (2024). https://doi.org/10.1002/zamm.202300475

[30] R.S. Nath, and R.K. Deka, "A numerical study on the mhd ternary hybrid nanofluid (cu-al2o3-tio2/h2o) in presence of thermal stratification and radiation across a vertically stretching cylinder in a porous medium," East European Journal of Physics, (1), 232–242 (2024). https://doi.org/10.26565/2312-4334-2024-1-19

[31] M. Sheikholeslami, H.R. Kataria, and A.S. Mittal, "Effect of thermal diffusion and heat generation on mhd nanofluid flow past an oscillating vertical plate through porous medium," Journal of Molecular Liquids, **257**, 12–25 (2018). https://doi.org/10.1016/j.molliq.2018.02.079

[32] R. Rammoorthi, and D. Mohanavel, "Influence of radiative magnetic field on a convective flow of a chemically reactive hybrid nanofluid over a vertical plate," Journal of Advanced Research in Fluid Mechanics and Thermal Sciences, **105**(1), 90–106 (2023). https://doi.org/10.37934/arfmts.105.1.90106

[33] S. Rosseland, *Astrophysik und atom-theoretische Grundlagen*, (Springer-verlag, berlin, 1931).

[34] B. Carnahan, H.A. Luther, and J.O. Wilkes, *Applied numerical methods*, (john willey and sons. Inc., New York, 1969), pp. 168–169.

[35] V.M. Soundalgekar, and P. Ganesan, "Finite-difference analysis of transient free convection with mass transfer on an isothermal vertical flat plate," International Journal of Engineering Science, **19**(6), 757–770 (1981). https://doi.org/10.1016/0020-7225(81)90109-9

ЧИСЕЛЬНЕ ДОСЛІДЖЕННЯ ВПЛИВУ ТЕРМІЧНОЇ ТА МАСОВОЇ СТРАТИФІКАЦІЇ НА ХІМІЧНО РЕАГУЮЧИЙ НЕСТАЦІОНАРНИЙ МГД-ПОТІК НАНОФЛЮЇДУ ПОВЗ ОСЦИЛЮЮЧУ ВЕРТИКАЛЬНУ ПЛАСТИНУ ЧЕРЕЗ ПОРИСТЕ СЕРЕДОВИЩЕ

Хемант Агарвал[a], **Шьяманта Чакраборті**[b], **Рупам Шанкар Нат**[a]

[a] *Департамент математики, Університет Гаухаті, Гувахаті-781014, Ассам, Індія*

[b] *UGC-HRDC, Університет Гаухаті, Гувахаті-781014, Ассам, Індія*

Метою цього дослідження є вивчення спільного впливу термічної та масової стратифікації на нестаціонарну магнітогідродинамічну нанофлюїд повз вертикально коливальну пластину зі змінною температурою. Основні рівняння задачі розв'язуються чисельно за допомогою неявного підходу Кренка-Ніколсона. Значні результати термічної та масової стратифікації контрастують із середовищем, де стратифікація відсутня. Швидкість зменшується при обох типах стратифікації, тоді як температура зменшується при термічній стратифікації, а концентрація зменшується при масовій стратифікації. Ми використовуємо графіки, щоб продемонструвати вплив різних параметрів, у тому числі фазового кута, теплового випромінювання, напруженості магнітного поля, джерел тепла/стікача та хімічних реакцій. Крім того, обчислюються та представлені графічно коефіцієнт шкірного тертя, число Нуссельта та число Шервуда. Результати підкреслюють критичну роль стратифікації в покращенні динаміки рідини та підвищенні ефективності процесів тепло- та масообміну, надаючи важливу інформацію для інженерних та екологічних застосувань за подібних обставин.

Ключові слова: *стратифікація маси; хімічна реакція; нанофлюїд; термічна стратифікація; осцилююча вертикальна пластина; метод Кренка-Ніколсона; теплове випромінювання; пористе середовище; МГД*